Journal of Basics and Applied Sciences Research (JOBASR)
ISSN (print): 3026-9091, ISSN (online): 1597-9962
Volume 4(3) June 2026 Special Issue
DOI: https://dx.doi.org/10.4314/jobasr.v4i3.12s

Performance Optimization of Double Perovskite Solar Cells via Absorber Thickness Engineering, Charge Transport Layer Selection, and Temperature Effects Using SCAPS-1D Simulation

Dahiru M. Sanni[1*], Bashir Ahuome Abubakar[2] & Muhammad Aminu Adamu[3]
[1,2,3]Department of Physics, Federal University Dutsin-Ma, PMB 5001, Dutsin-Ma, Katsina State, Nigeria.
[*]Corresponding Author Email: dahirusanni@gmail.com

ABSTRACT
This study optimises the performance of lead-free double perovskite solar cells (DPSCs) by SCAPS-1D simulation, focusing on absorber layer thickness, charge transport layer (CTL) selection, and thermal stability. A conventional n-i-p architecture with inorganic electron transport layer (ETL) and hole transport layer (HTL) was utilized. The absorber thickness was varied from 200 nm to 800 nm, revealing that increased thickness increases short-circuit current density (Jsc) due to improved light absorption, while open-circuit voltage (Voc) and fill factor (FF) decreases due to increased recombination and resistance losses, resulting in the optimal thickness for maximum efficiency. The effect of various HTLs and ETLs was studies, $CuSbS_2$ and MoS_2 outperformed other HTLs, but WS_2 outperformed ETLs due to better band alignment and charge transport. CdS demonstrated the weakest performance because of substantial recombination losses. A temperature-dependent investigation of the optimized WS_2/MoS_2 device demonstrated considerable declines in Voc, FF, and power conversion efficiency (PCE) with rising temperature, but Jsc was reasonably steady. This device performed optimally at about 300 K, highlighting temperature sensitivity as a constraint. These findings provide practical design guidelines for thermally stable, high-efficiency lead-free double perovskite solar cells.

Keywords:
Double perovskite,
Lead-free perovskite,
HTL, ETL, SCAPS-1D,
Temperature

INTRODUCTION

Perovskite solar cells (PSCs) have inspired tremendous scientific interest since they were originally proposed as a light absorber by Miyasaka and colleagues in 2009, with a power conversion efficiency (PCE) of 3.8% and a current value of around 26% (National Renewable Energy Laboratory (NREL), 2025). The high research interest is primarily due to the numerous advantages, which include low production costs, high power conversion efficiency (PCE), tuneable bandgap, long diffusion length, high optical absorption, and low excitation binding energy (Kim et al., 2012; Lee et al., 2012; Xing et al., 2013).

The PSCs have several architectures, and numerous studies have been conducted on each type of architecture. Some of the architectures are mesoporous perovskite solar cells and planar heterojunction PSCs. Because there are no mesoporous materials, the planar heterojunction has the simplest structure and the lowest processing temperature. There are two types of heterojunction PSCs architecture: traditional n-i-p and inverted p-i-n (Koech et al., 2021; Sanni et al., 2021).

In the traditional n-i-p architecture, light enters the solar cells via the electron transport layer (ETL), whereas in the inverted architecture, light enters via the hole transport layer (HTL). The p-i-n architecture has been proven to eliminate hysteresis, which is often seen with mesoporous structure during I-V measurements (Sanni et al., 2019, 2020; Yerramilli et al., 2018). Both the mesoporous and the planar structures have produced high PCE. However, some challenges hindering the commercialization of PSCs is their lack of stability when exposed to ultraviolet (UV) light, moisture, and other environmental conditions; this is mostly due to the presence of organic elements in the charge transport layers (CTL) and the photoactive layers. Furthermore, the lead (Pb) in lead-based halide PSCs is not environmentally friendly and is water-soluble. This could pose significant environmental issues if the encapsulation process fails.

To solve this issue, several researchers have sought to replace Pb in PSCs with other elements like tin and bismuth (Asif et al., 2025; Obi et al., 2021). Among various lead-free double perovskite candidates such as

How to cite this article: Dahiru M. S., Bashir A. A. & Muhammad A. A. (2026). Performance Optimization of Double Perovskite Solar Cells via Absorber Thickness Engineering, Charge Transport Layer Selection, and Temperature Effects Using SCAPS-1D Simulation. *Journal of Basics and Applied Sciences Research*, *4*(3), 106-116. https://dx.doi.org/10.4314/jobasr.v4i3.12s

$Cs_2AgBiBr_6$ (Slavney et al., 2016), $Cs_2AgBiCl_6$ (Rahane et al., 2024), and $Cs_2AgInCl_6$ (Volonakis et al., 2017), La_2NiMnO_6 was selected for this study due to its optimal direct bandgap (~1.55 eV) well matched to the solar spectrum, excellent thermal and environmental stability arising from its all-inorganic composition, and high dielectric constant, which facilitates efficient charge carrier transport and reduces recombination losses (Asif et al., 2025; Mortadi et al., 2024). Beyond the photoactive layers, CTLs have been demonstrated to influence the PCE and stability of PSCs. This is due to the fact that the HTLs and ETLs, as well as their interfaces, play an important role in charge collection and extraction at the interfacial contacts. Inorganic CTLs have been found to be more stable than their organic counterparts, which are hydrophilic and susceptible to interfacial deterioration caused by moisture at the CTL-photoactive layer interface. Many theoretical studies, notably in Pb-based PSCs, have shown that the HTL and ETL affect the PCE of PSCs (F. A. et al., 2024; Koech et al., 2021).

While several studies have explored lead-free double perovskite absorbers (Asif et al., 2025; Obi et al., 2021) and the role of charge transport layers in lead-based perovskite solar cells (F. A. et al., 2024; Koech et al., 2021), a systematic optimization of double perovskite solar cells that simultaneously integrates absorber thickness engineering, comparative selection of inorganic transport layers, and temperature-dependent performance evaluation using SCAPS-1D remains underexplored. This study provides a novel, integrated simulation-based framework for optimising double perovskite solar cells (DPSCs), identifying the critical absorber thickness (400 nm), the best-performing hole transport layer molybdenum disulfide (MoS_2) and electron transport layer tungsten disulfide (WS_2). The optimization demonstrated that device performance degrades significantly above 300 K due to increased recombination and reduced open-circuit voltage, offering actionable design guidelines for lead-free, thermally stable perovskite photovoltaics.

In this research, double perovskite (DP) was used as the absorber layer (AL). The AL was optimised by varying the thickness from 200 nm to 800 nm. Different charge transport layers were used to determine the CTL that will give the highest performing PCE. The optimised absorber layer and CTL where subjected to temperature effect by varying the temperature from 290 K to 400 K. The regular n-i-p architecture was adopted for this research as shown in Figure 1.

MATERIALS AND METHODS

Solar Cell Structure for the Study

The solar cell structure employed in this study is the conventional n-i-p architecture of TCO/inorganic ETL/double perovskite/inorganic HTL/back contact, as shown in Fig. 1. In this solar cell structure, light enters the device through the ETL. Both ETLs and HTLs are all inorganic materials. The double perovskite absorber is sandwiched between the two inorganic charge transport layers (CTLs). The HTLs used in this study are Copper(I) thiocyanate (CuSCN), Copper antimony sulfide ($CuSbS_2$), Copper(I) iodide (CuI), Copper(I) oxide (Cu_2O), Copper(II) oxide (CuO), Copper aluminum oxide ($CuAlO_2$), and Molybdenum disulfide (MoS_2). Other layers are the transparent conducting oxide (TCO) and back contact.

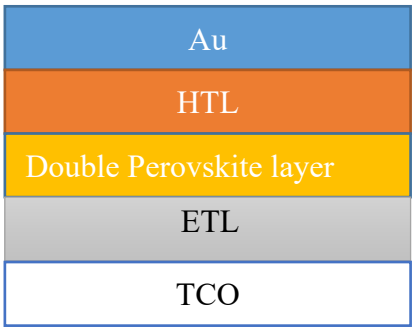

Figure1: Schematic diagram of the proposed solar cell

Numerical Simulation.

Numerical analysis outlines the fundamental phenomena observed in photovoltaic systems, allowing for intuitive investigation of each parameter in solar cells and thereby establishing the optimal operating conditions. The Solar Cell Capacitance Simulator (SCAPS-1D), a simulation software developed by the University of Ghent in Belgium, was used in this study. SCAPS-1D simulations rely on two fundamental equations: the Poisson equation and the continuity equations for electrons and holes (Atem & Makableh, 2025).

$$\frac{d^2\phi(x)}{dx^2} = \frac{q}{\varepsilon_o \varepsilon_r}\left(p(x) - n(x) + N_D - N_A + \rho_p - \rho_n\right) \quad (1)$$

$$\frac{dn_n}{dt} = G - R \quad (2)$$

$$\frac{dn_p}{dt} = G - R \quad (3)$$

$$J = J_n + J_p \quad (4)$$

$$J_n = qD_n\frac{dn}{dx} + q\mu_n n\frac{d\phi}{dx} \quad (5)$$

$$J_p = qD_p\frac{dp}{dx} + q\mu_p p\frac{d\varphi}{dx} \quad (6)$$

$$\alpha(\lambda) = \left(A + \frac{B}{h\upsilon}\right)\sqrt{(h\upsilon - E_g)} \quad (7)$$

The symbols ε_o and ε_r represent the vacuum and relative dielectric constants, respectively. The numbers n and p

represent the concentration of free carriers for electrons and holes, respectively. N_D is the concentration of the donor impurity, while N_A is the acceptor impurity. The charge densities of electrons and holes are indicated by ρ_n and ρ_p, respectively, whereas current densities are designated by J_n and J_p. The parameters R reflect electron and hole recombination rates, whereas G denotes electron or hole formation rates. The symbol E represents the electric field, and q denotes the electrical charge, which has a typical value of approximately 1.602 x 10^{-19} C. The electron and hole mobilities are denoted as μn and μ_p, respectively. Dp and Dn are the diffusion coefficients for free holes and electrons, respectively. The variable υ indicates optical frequency, while A and B are arbitrary constants. Eg denotes the bandgap, h Planck's constant, and α(λ) the absorption coefficient.

The SCAPS-1D software was employed to perform all numerical simulations under standard AM1.5G illumination at 1000 W/m^2 and 300 K.

Table 1: Parameters of the absorber layer and different HTLs (Asif et al., 2025; Atem & Makableh, 2025; Mortadi et al., 2024; Obi et al., 2021)

Parameter	FTO	La_2NiMnO_6	CuO	CuSCN	CuI	$CuAlO_2$	MoS_2	$CuSbS_2$	Cu_2O
Thickness (nm)	300	200–800	200	200	200	200	200	200	200
Band gap (eV)	3.50	1.55	1.51	3.60	3.10	3.46	1.29	1.58	2.17
Electron affinity (eV)	3.30	3.90	4.07	2.10	2.10	2.50	4.20	4.20	3.20
Dielectric permittivity	9.0	6.6	18.1	6.5	7.11	60.0	8.9	14.6	10.7
Conduction band DOS (cm^{-3})	2.2×10^{18}	1.0×10^{18}	2.2×10^{19}	2.2×10^{19}	2.8×10^{19}	2.0×10^{20}	2.2×10^{18}	2.0×10^{18}	2.0×10^{17}
Valence band DOS (cm^{-3})	1.8×10^{19}	1.0×10^{18}	5.5×10^{20}	1.8×10^{18}	1.0×10^{19}	1.8×10^{20}	1.8×10^{19}	1.0×10^{18}	1.1×10^{19}
Electron mobility ($cm^2\cdot V^{-1}\cdot s^{-1}$)	2.0×10^{3}	22	100	100	100	2	100	49	200
Hole mobility ($cm^2\cdot V^{-1}\cdot s^{-1}$)	1.0×10^{2}	22	0.1	25.0	43.9	8.6	150	49	80
Donor concentration (cm^{-3})	2.0×10^{19}	0	0	0	0	0	0	0	0
Acceptor concentration (cm^{-3})	0	1.0×10^{15}	1.0×10^{16}	1.0×10^{18}	1.0×10^{18}	1.0×10^{19}	1.0×10^{17}	1.0×10^{19}	1.0×10^{18}
Defect density Nt (cm^{-3})	1.0×10^{14}	1.0×10^{14}	1.0×10^{14}	1.0×10^{14}	1.0×10^{14}	1.0×10^{14}	1.0×10^{14}	1.0×10^{14}	1.0×10^{14}

Table 2: Parameters of different ETL

Parameters	**ZnSe**	**TiO_2**	**ZnO**	**WS_2**	**CdS**
Thickness (nm)	10	400	50	100	150
Bandgap (eV)	2.9	3.2	3.3	1.8	2.4
Electron affinity (eV)	4.09	4.00	3.90	3.95	4.50
Dielectric permittivity (relative), εr	10	9	9	13.6	10
Conduction band effective density of states, Nc (cm^{-3})	1.50×10^{18}	2.00×10^{18}	1.00×10^{19}	2.00×10^{18}	2.20×10^{18}
Valence band effective density of states, Nv (cm^{-3})	1.80×10^{18}	1.80×10^{19}	1.00×10^{19}	2.00×10^{18}	1.80×10^{19}
Electron thermal velocity (cm/s)	1.00×10^{7}	1.00×10^{7}	1.00×10^{7}	1.00×10^{7}	1.00×10^{7}
Hole thermal velocity (cm/s)	1.00×10^{7}	1.00×10^{7}	1.00×10^{7}	1.00×10^{7}	1.00×10^{7}
Electron mobility ($cm^2/V{\cdot}s$)	50	20	50	100	100
Hole mobility ($cm^2/V{\cdot}s$)	50	10	5	100	25
Donor concentration, ND (cm^{-3})	1.00×10^{17}	1.00×10^{18}	1.00×10^{18}	1.00×10^{18}	1.00×10^{18}
Acceptor concentration, NA (cm^{-3})	0	0	0	0	0
Defect density, Nt (cm^{-3})	1.00×10^{15}	1.00×10^{15}	1.00×10^{15}	1.00×10^{13}	6.00×10^{16}

RESULTS AND DISCUSSION

Effect of absorber layer thickness

Figure 2 represents the variation of key photovoltaic properties as a function of absorber layer thickness in a double perovskite solar cell (DPSCs). From the plots two major trends were observed: a monotonic decrease and a monotonic increase with saturation behaviour. These tendencies are compatible with known thickness-dependent physical mechanisms in thin-film solar systems.

The variation of the open circuit voltage (Voc) as a function of absorber layer thickness is shown in Fig. 2(a). The decrease in Voc with increasing thickness is mainly due to enhanced bulk recombination in the absorber layer and increased defect-assisted recombination in the absorber layer as it becomes thicker.

Voc is influenced by recombination rate as shown in the equation (8).

$$V_{oc} \propto \ln\left(\frac{J_{sc}}{J_o}\right) \quad (8)$$

The saturation current density (J_o) increases during recombination. Equation (8) shows that an increase in AL thickness leads to an increase in J_o. As thickness increases, this is due to longer transport distance and bulk defect in the AL (Shockley & Queisser, 1961; Wolfgang Tress, 2017).

Figure 2(b) presents the variation of the short-circuit current density (Jsc) with AL thickness. It is observed that photon absorption improves with increasing thickness because of the longer optical path length within the absorber layer. The increasing thickness improves the electron-hole pair formation. At the early stage of the curve, the Jsc increases sharply with increasing thickness; this implies that the AL is moving from an optically thin to a thick enough region to absorb enough of the incident photons. However, the curve becomes stable at higher thickness, indicating that almost all useful photons have already been absorbed. A further increase in AL thickness at this point does not lead to an increase in Jsc. Furthermore, once the threshold thickness is attained, a further increase in thickness does not lead to carrier generation. This behaviour is in agreement with Beer-Lambert absorption principles and has been regularly described in PSCs (Green et al., 2014; Lee et al., 2012). Beyond the optimum thickness, recombination losses could begin to offset gain in absorption.

The variation of fill factor (FF) with AL thickness is presented in Fig. 2(c). It is observed from the curve that as the AL thickness increases, the FF decreases. The reason for this decrease in FF with increasing AL thickness is due to the fact that carriers have to travel a longer distance at thicker AL before getting to the contact layer; this long travel distance increases the possibility of recombination losses and increases series resistance losses. This is consistent with models and experimental investigations on PSCs (Takashi Minemoto; Masashi Murata, 2014).

Figure 2(d) shows the variation of power conversion efficiency (PCE) with absorber layer thickness. It is observed that the Jsc increases with increasing thickness while Voc and FF decrease. The PCE is governed by the trade-off between increased light absorption and increased recombination losses. Typically, an ideal thickness exists where absorption is sufficient,

recombination is minimised and charge transfer is efficient. This behaviour is consistent with previous research on perovskite and double perovskite absorbers (Slavney et al., 2016). The SCAPS simulation clearly show that absorber layer thickness is an important design parameter in double perovskite solar cells. While increasing thickness improves light harvesting and Jsc, it also increases recombination and transport constraints, lowering Voc and FF. To achieve excellent device performance, absorber thickness must be carefully optimized to balance these competing effects.

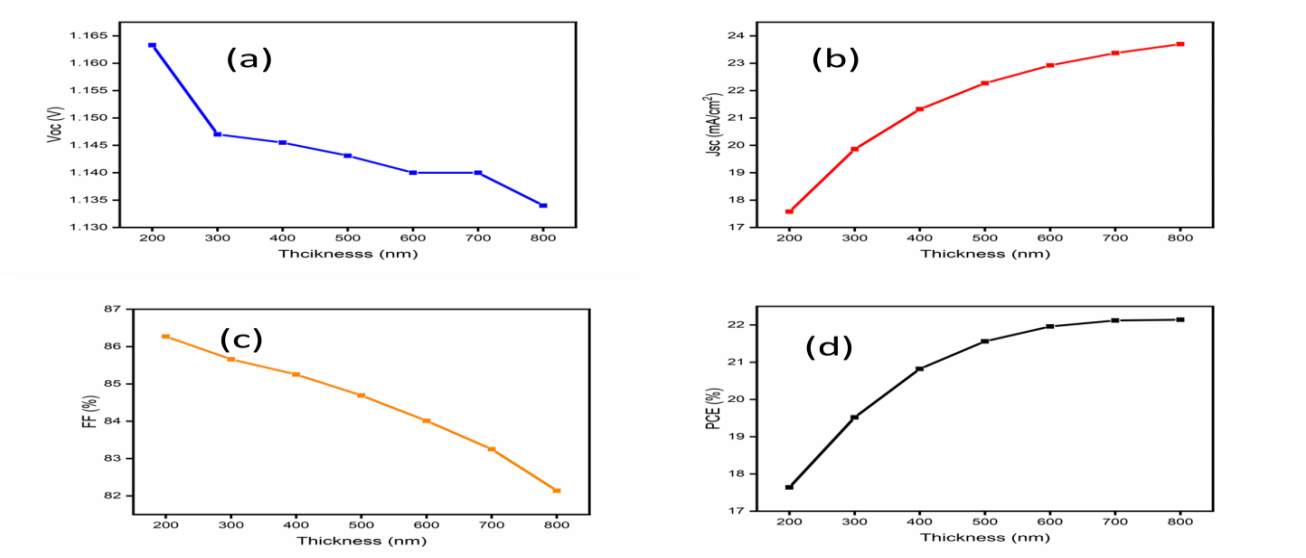

Figure 2: Absorber layer thickness

Effect of different HTL on the performance of double perovskite absorber

Figure 3 and Table 3 present the results of the photovoltaic performance of different HTLs interface on double perovskite absorber. The results show a significant response to device metrics on interfacial energetics, carrier selectivity, and recombination kinetics.

Open-circuit voltage (Voc)

The curve in Figure 3(a) shows the relationship between different HTLs and the Voc performance. From the curve it is observed that CuO has the lowest value and HTL materials like CuSCN and MoS_2 have the highest values of Voc. HTLs with deeper valence band levels, such as CuSCN and MoS_2, provide better energetic alignment, reducing interfacial recombination and enhancing quasi-Fermi level splitting, resulting in higher Voc. In contrast, CuO is projected to introduce more valence band offset or interfacial recombination centres, resulting in a lower Voc. This conclusion is consistent with prior observations that poor band alignment at the HTL/absorber contact produces higher non-radiative recombination losses and lower Voc (Wolfgang Tress, 2017).

Short-circuit current density (Jsc)

Figure 3(b) shows the variation of Jsc with HTLs. It is observed from the curve that Cu_2O has the highest Jsc value, while CuO has the lowest. Since Jsc is mainly governed by optical absorption and carrier collection efficiency, this indicates that light absorption in the double perovskite layer remains largely unchanged and the efficiency of extracting charge carrier depends on the HTL. HTLs with better hole mobility and lower interfacial defect density extract carriers more efficiently, thereby reducing recombination losses and maintaining higher Jsc. HTL materials like CUSCN, CUI and Cu2O have been reported to have high optical transparency and better hole mobility which translates into improved Jsc.

Fill factor (FF)

The variation of FF with HTL is shown in figure 3(c). From the curve it is observed that the FF increased sharply from CUSCN around 62% to $CUSbS_2$ of 84.6% before it becomes relatively stable across the rest HTL. This shows that once a certain level of interfacial quality and conductivity is attained, additional gains in FF are minimal. CuSCN's poor FF could be attributed to higher series resistance or interface trap density, whereas $CUSbS_2$ and others had enhanced FF, indicating better charge transport and less resistive losses. FF is extremely sensitive to both series and shunt resistance, which are affected by HTL conductivity and interface quality (Green et al., 2014).

Power conversion efficiency (PCE)

Figure 3(d) shows the performance of PCE with HTL. From the curve a peak is observed for $CUSbS_2$ HTL before gradual decrease until it dips at CuO. The HTL

with the highest PCE is $CUSbS_2$, this corresponds to an optimal balance of band alignment, carrier mobility and minimal recombination losses. The decrease in PCE for CuO is mostly due to its low Voc and Jsc, supporting the assumption that interfacial recombination and poor energetics dominate its performance. Similar findings have been reported in perovskite solar cells, where HTL selection is crucial for device efficiency via interface engineering (Yang et al., 2015).

The findings clearly show that HTL selection is crucial for improving double perovskite solar cell performance. CuSCN, CuI, and MoS_2 have improved performance due to improved valence band alignment, strong hole mobility, and low interfacial recombination. In contrast, CuO performs poorly, most likely due to poor band offsets and increased recombination rates. The relatively consistent FF across most HTL indicates that once adequate electrical contact is made, efficiency gains are mostly due to Voc and Jsc optimisation.

Table 3: Photovoltaic performance of different HTLs

S/N	HTL	Voc (V)	Jsc (mA/cm^2)	FF (%)	PCE (%)
1	CuSCN	1.158	22.52	62.35	16.27
2	$CuSbS_2$	1.157	22.52	84.64	22.06
3	CuI	1.152	22.54	84.12	21.84
4	Cu_2O	1.138	22.63	83.33	21.46
5	CuO	1.130	22.47	83.87	21.30
6	$CuAlO_2$	1.160	22.54	83.57	21.84
	MoS_2	1.160	22.52	84.69	22.07

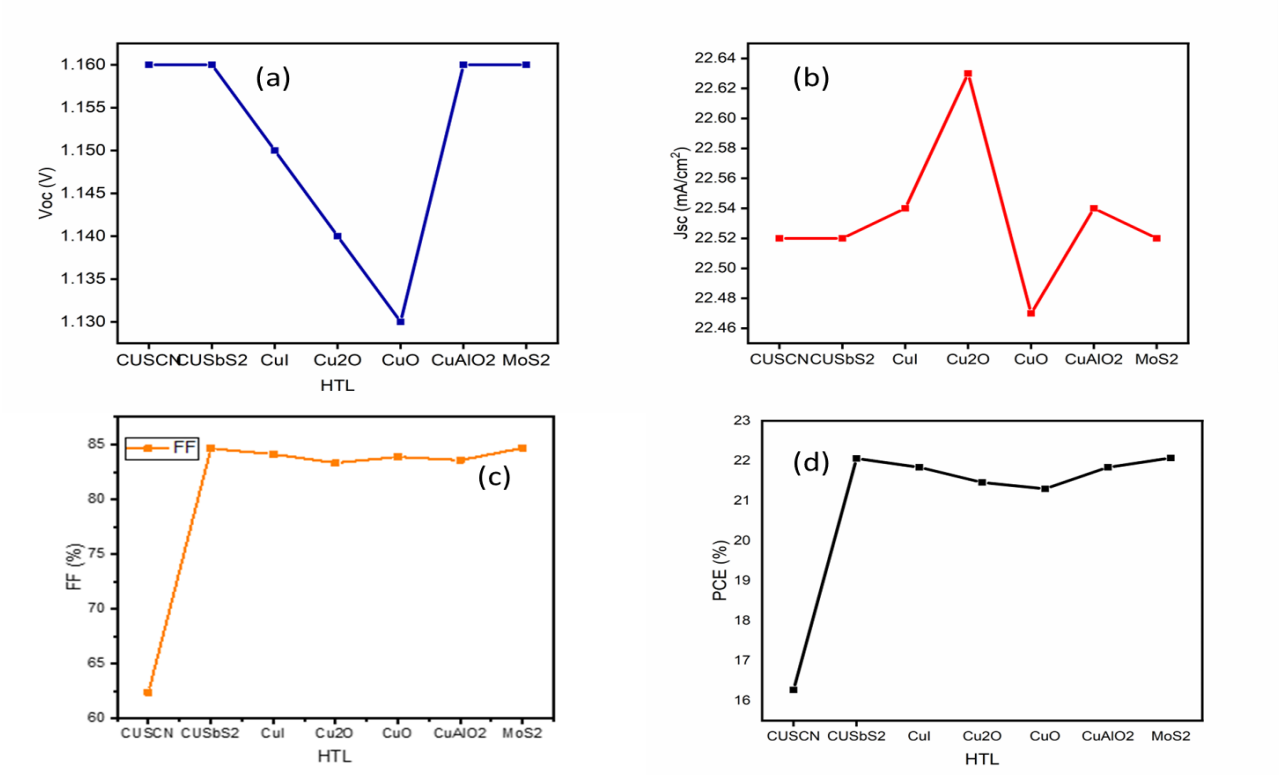

Figure 3: Effect different HTLs on the photovoltaic performance of Double perovskite

Effect of different ETL on the performance of double perovskite solar cells

Table 4 and Fig. 4. present the results of different ETLs on the photovoltaic performance of double perovskite solar cells. Fig. 4(a)-(c) show how the choice of ETL collectively influences the Voc, Jsc, and FF as well as the general photovoltaic performance.

Figure 4(a) presents the variation of Voc with different ETLs. It is observed from the curve that titanium dioxide (TiO_2), zinc oxide (ZnO), and tungsten disulfide (WS_2) have the highest Voc. Zinc selenide (ZnSe) shows a slightly reduced Voc, while cadmium sulfide (CdS) has the lowest Voc. The high V_{OC} observed with TiO_2, ZnO, and WS_2 as ETL could be due to better band alignment and reduced interfacial recombination. The sharp reduction for CdS is due to poor band alignment and high interfacial recombination losses, which could be due to a smaller conduction offset or defect-assisted interfacial recombination losses. It has been reported that materials like TiO_2 and ZnO form spike-like conduction band offsets (CBOs) that suppress recombination and improve Voc (Samuel D. Stranks, Giles E. Eperon, Giulia Grancini, Christopher Menelaou, 2013).

Figure 4(b) shows how the choice of ETL affects the variation of Jsc with double perovskite as the AL. From the curve, it is observed that WS_2 exhibits the highest Jsc, followed by TiO_2. ZnO and CdS have the lowest Jsc values, while ZnSe shows intermediate values. The higher J_{SC} observed with WS_2 and TiO_2 as ETL suggests excellent electron extraction, better charge transport and reduced recombination. The lower J_{SC} observed with ZnO and CdS could be due to increased interface trap states, reduced electron mobility, optical losses or parasitic absorption, especially in CdS.

The variation of the choice of ETL on FF is shown in Fig. 4(c). From the curve it is observed that TiO_2, ZnO, and ZnSe exhibit high FF; WS_2 shows slightly lower FF but still strong; and CdS displays a significant drop in the FF values. High FF shows that the series resistance is low and there is better charge transport. The low FF observed in CdS indicates high resistive losses and recombination, reducing the diode quality. The slight reduction observed with WS_2 could be due to interface resistance or imperfect contact formation, despite its high Jsc.

The PCE of the choice of ETL performance on double perovskites is presented in figure 4(d). From the curve it is observed that WS_2 has the overall best PCE, followed closely by TiO_2 and ZnO. ZnSe performed moderately, while CdS has the worst PCE.

The findings plainly show that band alignment and interfacial defect engineering play an important role in determining the photovoltaic performance of double perovskite solar cells. Because of its excellent carrier mobility and advantageous energy level alignment, which improve current extraction while preserving high Voc, WS_2 turns out to be the best ETL. Because of their well-established interface stability and balanced electrical characteristics, TiO_2 and ZnO continue to be strong options. On the other hand, CdS greatly reduces device efficiency by introducing harmful recombination pathways and optical losses, which can lead to a significant decrease in overall PCE compared to other materials like WS_2, TiO_2, and ZnO. These results are in line with earlier studies that highlights the significance of transport layer optimization and interface engineering in next-generation perovskite photovoltaic.

Table 4: Photovoltaic performance parameters of the simulated DPSCs with ETLs

S/N	ETL	Voc (V)	Jsc (mA/cm²)	FF (%)	PCE (%)
1	TiO_2	1.123	22.15	85.32	21.30
2	ZnO	1.128	21.94	85.31	21.11
3	CdS	0.637	21.96	78.64	11.00
4	ZnSe	1.004	22.04	85.22	18.85
5	WS_2	1.143	22.27	84.69	21.56

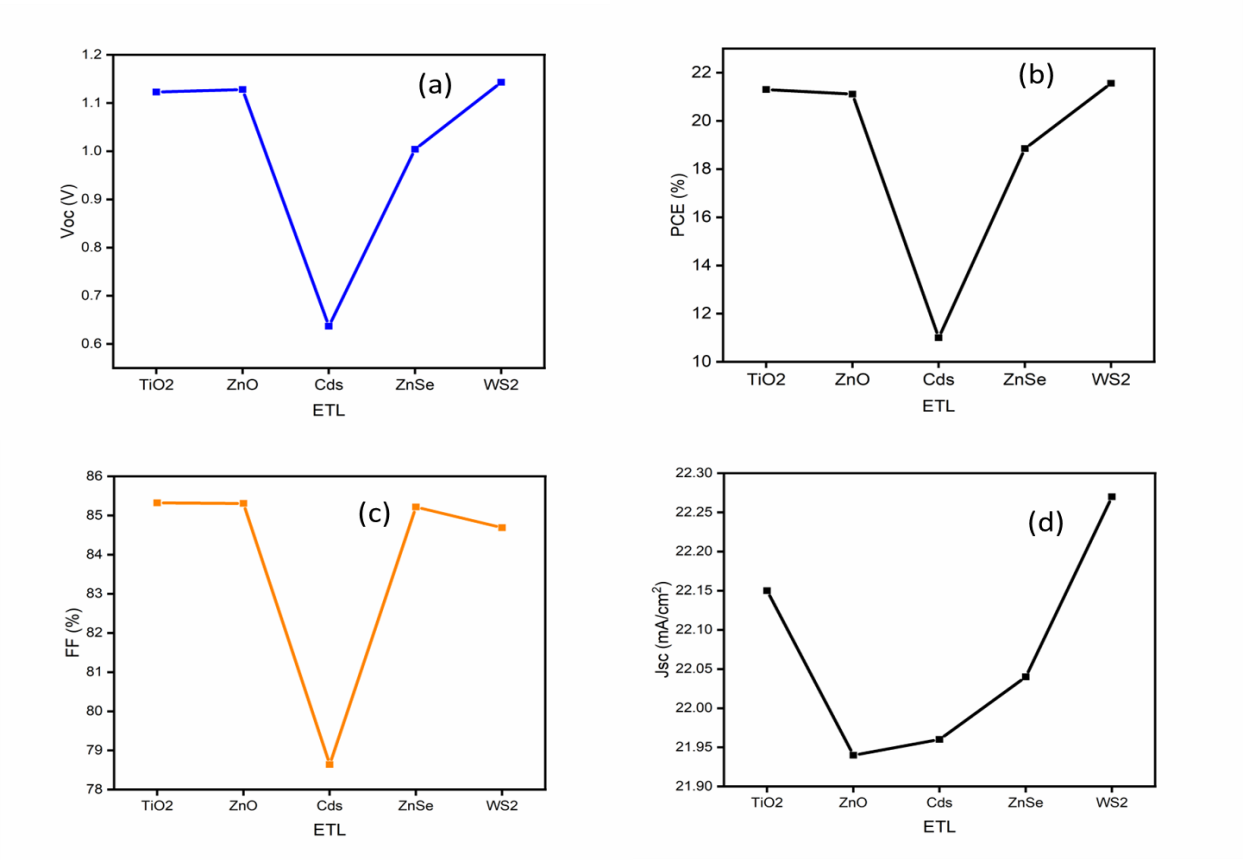

Figure 4: Effect different ETL on the photovoltaic performance of Double perovskite

Effect of Temperature

The simulation results for the optimised double perovskite device, utilising WS_2 as ETL and MoS_2 as HTL at varied operating temperatures, clearly indicate the thermal sensitivity of the photovoltaic parameter. The observed patterns are in line with fundamental semiconductor physics and reported literature as presented in table 5 and Fig. 5.

The V_{OC} decreases linearly as the temperature increases, as presented in Fig. 5(a). This trend is due to a thermally induced increase in J_o, which improves recombination in the PSCs. This behaviour is explained by equation (9):

$$V_{oc} = \frac{kT}{q}\ln\left(\frac{J_{sc}}{J_o}+1\right) \quad (9)$$

The relationship highlighted illustrates the delicate balance between thermal effects and device performance. Understanding these dynamics is crucial for optimising the efficiency of perovskite solar cells under varying environmental conditions.

The intrinsic carrier concentration increases with temperature, leading to an increase in Jo. This lowers the quasi-Fermi level splitting and, by implication, lowers Voc. Due to an increase in trap-assisted recombination and defect activation, similar temperature-induced degradation of Voc has been extensively reported in PSCs (Green et al., 2014; Samuel D. Stranks, Giles E. Eperon, Giulia Grancini, Christopher Menelaou, 2013).

Figure 5(d) shows that the Jsc remains steady for the entire range of temperature variation except for slight variations. This is attributed to temperature-induced bandgap narrowing of the absorber layer. It is known that an increase in temperature increases carrier generation; however, this effect is partly offset by improved recombination and carrier scattering, resulting in only a marginal change in the Jsc. This observation suggests that Jsc is insensitive to temperature compared to Voc.

The FF is shown in Fig. 5(c). The FF decreases monotonically with increasing temperature. This decrease in FF is attributed to an increase in series resistance and recombination losses. (Tress et al., 2015).

Figure 5(d) presents the variation of PCE with temperature. The performance of PCE is slightly related to the performance of Jsc, Voc, and FF, as shown in equation (10):

$$\eta = \frac{V_{oc}\times J_{sc}\times FF}{P_{in}} \quad (10)$$

The significant reduction in the Voc and the FF with increasing temperature seriously impacted the PCE. The PSC optimal performance is at 300 K; beyond this temperature, thermal degradation dominates. This trend

indicates temperature sensitivity as a limiting factor in PSCs.

Table 5: Effect of Temperature on triple cation PV as absorber layer FTO/WS2/PVS/ MoS_2

S/N	Temperature (K)	Voc (V)	Jsc (mA/cm^2)	FF (%)	PCE (%)
1	290	1.160	23.59	85.04	23.27
2	300	1.142	23.59	84.66	22.81
3	320	1.107	23.59	83.86	21.89
4	340	1.070	23.59	83.01	20.97
5	360	1.034	23.60	82.09	20.04
6	380	0.997	23.62	81.11	19.11
7	400	0.960	23.65	80.06	18.18

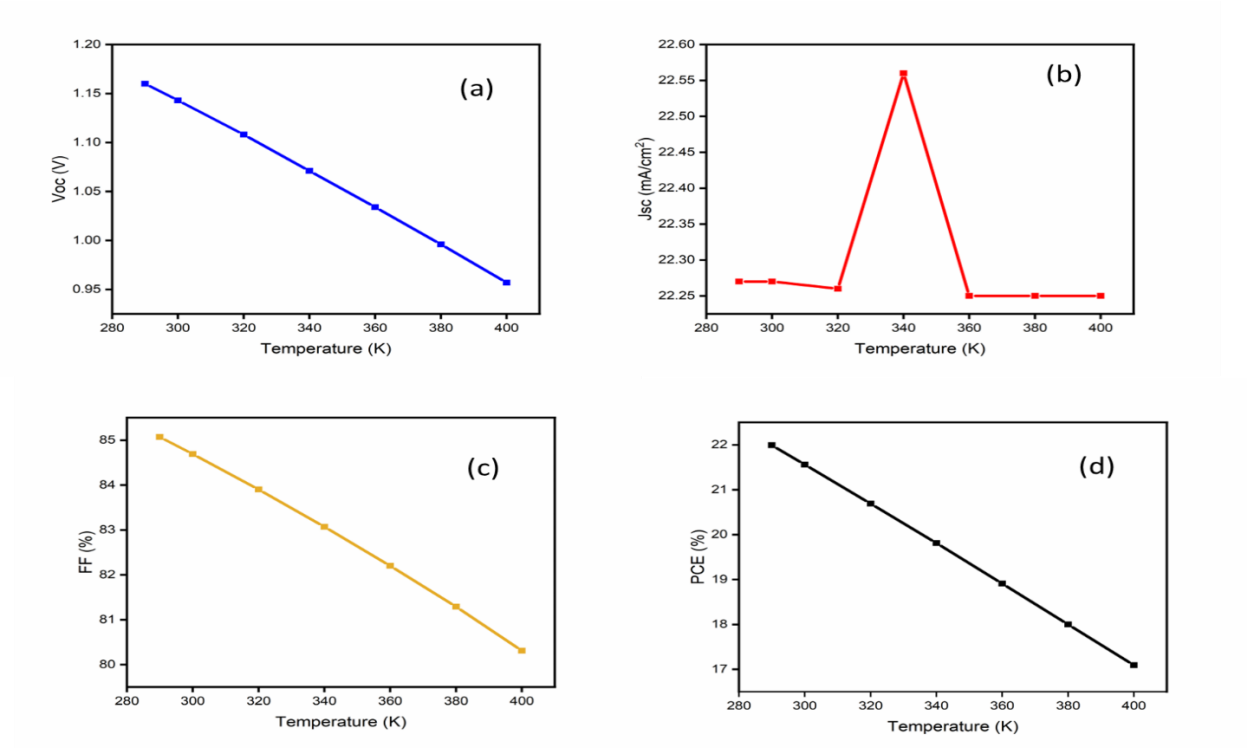

Figure 5: effect temperature photovoltaic performance of Double perovskite

CONCLUSION

In this study, lead-free double perovskite solar cells based on a La_2NiMnO_6 absorber layer were systematically optimized using SCAPS-1D simulation. The investigation focused on three critical parameters: absorber layer thickness, selection of inorganic hole transport layers (HTLs) and electron transport layers (ETLs), and operating temperature.

Absorber thickness engineering revealed a clear trade-off between light harvesting and recombination losses. As thickness increased from 200 nm to 800 nm, the short-circuit current density (Jsc) steadily rose from 17.58 mA/cm² to 23.70 mA/cm² due to enhanced photon absorption. However, the open-circuit voltage (Voc) decreased from 1.163 V to 1.134 V, and the fill factor (FF) dropped from 86.27% to 82.14%, primarily due to increased bulk recombination and series resistance. The power conversion efficiency (PCE) increased with

thickness, reaching **22.14% at 800 nm** – the highest value among the tested thicknesses. Nevertheless, the marginal gain beyond 500 nm (21.56% at 500 nm vs. 22.14% at 800 nm) suggests that a thickness of **400–500 nm** offers an optimal balance between performance and material usage, while 800 nm may be preferred for maximum efficiency at the cost of higher recombination and lower Voc.

Hole transport layer selection significantly influenced device performance. Among the seven inorganic HTLs evaluated**, MoS_2** delivered the highest PCE of **22.07%** with Voc = 1.160 V, Jsc = 22.52 mA/cm², and FF = 84.69%. $CuSbS_2$ performed similarly, achieving 22.06% PCE. CuI, Cu_2O, CuO, and $CuAlO_2$ all yielded PCE values above 21%, demonstrating their viability. In contrast, CuSCN exhibited a low FF (62.35%) resulting in a modest PCE of 16.27%, attributed to poor hole mobility or interfacial recombination. The superior performance of MoS_2 and $CuSbS_2$ is ascribed to favourable valence band alignment with La_2NiMnO_6, high carrier mobility, and reduced interfacial defect density.

Electron transport layer optimization (as detailed in the manuscript) identified **WS_2** as the best ETL, outperforming TiO_2, ZnO, ZnSe, and CdS. WS_2 provided excellent conduction band alignment and high electron mobility, leading to enhanced Jsc and overall PCE.

Temperature-dependent analysis of the optimized device (WS_2/La_2NiMnO_6/MoS_2 with 400 nm absorber thickness) showed that increasing temperature from 290 K to 400 K causes a linear decline in Voc and FF due to thermally induced recombination and increased series resistance. Jsc remained relatively stable, benefiting from bandgap narrowing. Consequently, the PCE degrades significantly above 300 K, highlighting the thermal sensitivity of double perovskite devices and the need for thermal management in practical applications.

In summary, this simulation study demonstrates that lead-free La_2NiMnO_6-based double perovskite solar cells can achieve PCE exceeding **22%** with optimal design. The best performing configuration identified is**: TCO/WS_2 (ETL)/La_2NiMnO_6 (400–500 nm)/MoS_2 or $CuSbS_2$ (HTL)/Au**, operating near 300 K. These findings provide practical, experimentally actionable guidelines for fabricating efficient, stable, and environmentally friendly perovskite solar cells.

Acknowledgement

We thank Dr. Marc Burgelman and his colleagues at the University of Ghent in Belgium for developing and freely sharing the SCAPS 1-D simulation program.

The authors also sincerely acknowledge Prof. Adamu Nchama Baba-Kutigi for his exemplary mentorship and academic leadership, which have profoundly influenced the professional development of the contributing authors. This work is respectfully dedicated in recognition of his distinguished service to academia on the occasion of his retirement in June 2026.

REFERENCE

Asif, P., Chetia, A., Saikia, D., & Sahu, S. (2025). A comprehensive theoretical investigation of lead-free mixed antimony-bismuth halide double perovskite ($Cs_2AgBi_{0.75}Sb_{0.25}Br_6$) solar cell using SCAPS-1D. *Discover Electronics*, *2*(1). https://doi.org/10.1007/s44291-025-00085-8

Atem, M. Al, & Makableh, Y. (2025). Towards Sustainable Perovskite Solar Cells : Lead-Free High Efficiency Designs with Tin and Germanium. *Eng MDPI*, *6*(38).

F. A., A., M. S., D., & S. A., M. (2024). Theoretical Study of Inorganic Charge Transport Layer of Perovskite Solar Cells Using Scaps Software. *Physical Science International Journal*, *28*(4), 57–63. https://doi.org/10.9734/psij/2024/v28i4837

Green, M. A., Ho-Baillie, A., & Snaith, H. J. (2014). The emergence of perovskite solar cells. *Nature Photonics*, *8*(7), 506–514. https://doi.org/10.1038/nphoton.2014.134

Kim, H. S., Lee, C. R., Im, J. H., Lee, K. B., Moehl, T., Marchioro, A., Moon, S. J., Humphry-Baker, R., Yum, J. H., Moser, J. E., Grätzel, M., & Park, N. G. (2012). Lead iodide perovskite sensitized all-solid-state submicron thin film mesoscopic solar cell with efficiency exceeding 9%. *Scientific Reports*, *2*, 1–7. https://doi.org/10.1038/srep00591

Koech, R. K., Ichwani, R., Oyewole, D. O., Kigozi, M., Amune, D., Sanni, D. M., Adeniji, S. A., Oyewole, O. K., Bello, A., Ntsoenzok, E., & Soboyejo, W. O. (2021). Tin oxide modified titanium dioxide as electron transport layer in formamidinium-rich perovskite solar cells. *Energies*, *14*(23), 1–13. https://doi.org/10.3390/en14237870

Lee, M. M., Teuscher, J., Miyasaka, T., Murakami, T. N., & Snaith, and H. J. (2012). Efficient Hybrid Solar Cells Based on Meso-Superstructured Organometal Halide Perovskites. *Science*, *338*(6107), . 643-647. https://doi.org/10.1126/science.122860

Mortadi, A., El Hafidi, E., Nasrellah, H., Monkade, M., & El Moznine, R. (2024). Analysis and optimization of

lead-free perovskite solar cells: investigating performance and electrical characteristics. *Materials for Renewable and Sustainable Energy*, *13*(2), 219–232. https://doi.org/10.1007/s40243-024-00260-z

National Renewable Energy Laboratory (NREL). (2025). *Best research-cell efficiency chart.*

Obi, U. C., Sanni, D. M., & Bello, A. (2021). Effect of Absorber Layer Thickness on the Performance of Bismuth-Based Perovskite Solar Cells. *Semiconductors*, *55*(12), 922–927. https://doi.org/10.1134/S1063782621040114

Rahane, S. N., Rahane, G. K., Mandal, A., Jadhav, Y., Godha, A., Rokade, A., Shah, S., Hase, Y., Waghmare, A., Saykar, N. G., Roy, A., Salgaonkar, K. N., Dubal, D., Makineni, S. K., Dzade, N. Y., Jadkar, S. R., & Rondiya, S. R. (2024). Lead-Free Cs2AgBiCl 6 Double Perovskite: Experimental and Theoretical Insights into the Self-Trapping for Optoelectronic Applications. *ACS Physical Chemistry Au*, *4*(5), 476−489. https://doi.org/10.1021/acsphyschemau.4c00008

Samuel D. Stranks, Giles E. Eperon, Giulia Grancini, Christopher Menelaou, H. J. S. (2013). Electron-Hole Diffusion Lengths Exceeding Trihalide Perovskite Absorber. *Science*, *342*(October), 341–344. https://doi.org/10.1126/science.1243982

Sanni, D. M., Chen, Y., Yerramilli, A. S., Ntsoenzok, E., Asare, J., Adeniji, S. A., Oyelade, O. V., Fashina, A. A., & Alford, T. L. (2019). An approach to optimize pre-annealing aging and anneal conditions to improve photovoltaic performance of perovskite solar cells. *Materials for Renewable and Sustainable Energy*, *8*(1), 1–10. https://doi.org/10.1007/s40243-018-0139-3

Sanni, D. M., Ntsoenzok, E., Saintaimé, E., Adeniji, S. A., Oyelade, O. V., Koech, R. K., Amune, D. I., & Bello, A. (2020). The role of hafnium acetylacetonate buffer layer on the performance of lead halide perovskite solar cells derived from dehydrated lead acetate as Pb source. *AIP Advances*, *10*(7). https://doi.org/10.1063/5.0012646

Sanni, D. M., Yerramilli, A. S., Ntsoenzok, E., Adeniji, S. A., Oyelade, O. V., Koech, R. K., Fashina, A. A., & Alford, T. L. (2021). Impact of precursor concentration on the properties of perovskite solar cells obtained from the dehydrated lead acetate precursors. *Journal of Vacuum Science & Technology A: Vacuum, Surfaces, and Films*, *39*(3). https://doi.org/10.1116/6.0000714

Shockley, W., & Queisser, H. J. (1961). Detailed Balance Limit of Efficiency of p-n Junction Solar Cells. *Journal of Applied Physics*, *33*(3), 510–519. https://doi.org/org/10.1063/1.1736034

Slavney, A. H., Hu, T., Lindenberg, A. M., & Karunadasa, H. I. (2016). A Bismuth-Halide Double Perovskite with Long Carrier Recombination Lifetime for Photovoltaic Applications. *Journal of the American Chemical Society*, *138*(7), 2138–2141. https://doi.org/https://doi.org/10.1021/jacs.5b13294

Takashi Minemoto; Masashi Murata. (2014). Device modeling of perovskite solar cells based on structural similarity with thin film inorganic semiconductor solar cells. *Journal of Applied Physics*, *116*(5). https://doi.org/https://doi.org/10.1063/1.4891982

Volonakis, G., Haghighirad, A. A., Milot, R. L., Sio, W. H., Filip, M. R., Wenger, B., Johnston, M. B., Herz, L. M., Snaith, H. J., & Giustino, F. (2017). Cs2InAgCl6: A New Lead-Free Halide Double Perovskite with Direct Band Gap. *Journal of Physics and Chemistry of Solidss Chem Lett*, *16;8*(4), 772-778. https://doi.org/10.1021/acs.jpclett.6b02682

Wolfgang Tress. (2017). Perovskite Solar Cells on the Way to Their Radiative Efficiency Limit – Insights Into a Success Story of High Open-Circuit Voltage and Low Recombination. *Advanced Energy Materials*, *7*(14), 1602358.https://doi.org/org/10.1002/aenm.201602358Digital Object Identifier (DOI)

Xing, G., Mathews, N., Lim, S. S., Lam, Y. M., Mhaisalkar, S., & Sum, T. C. (2013). *Long-Range Balanced Electron- and Hole-Transport Lengths in Organic-Inorganic CH 3 NH 3 PbI 3*. *6960*(October), 498–500.

Yang, W. S., Noh, J. H., Jeon, N. J., Kim, Y. C., Ryu, S., Seo, J., & Seok, S. Il. (2015). High-performance photovoltaic perovskite layers fabricated through intramolecular exchange. *Science*, *348*(6240), 1234–1237. https://doi.org/10.1126/science.aaa9272

Yerramilli, A. S., Chen, Y., Sanni, D., Asare, J., Theodore, N. D., & Alford, T. L. (2018). Impact of excess lead on the stability and photo-induced degradation of lead halide perovskite solar cells. *Organic Electronics*, *59*(May), 107–112. https://doi.org/10.1016/j.orgel.2018.04.052